Assembly of Bacteriophage Lambda Terminase into a Viral DNA Maturation and Packaging Machine†

Nasib Karl Maluf,‡,|| Hélène Gaussier,‡ Elke Bogner,⊥,# Michael Feiss,|| and Carlos Enrique Catalano*,‡,§

Department of Pharmaceutical Sciences and the Molecular Biology Program, University of Colorado Health Sciences Center, 4200 East Ninth Avenue C238, Denver, Colorado 80262, Department of Microbiology, University of Iowa, 51 Newton Road, Iowa City, Iowa 52242, and Institute of Clinical and Molecular Virology, Friedrich-Alexander University, Schlossgarten 4, 91054 Erlangen, Germany

Received July 26, 2006; Revised Manuscript Received October 6, 2006

ABSTRACT: Terminase enzymes are common to complex double-stranded DNA viruses and function to package viral DNA into the capsid. We recently demonstrated that the bacteriophage λ terminase gpA and gpNu1 proteins assemble into a stable heterotrimer with a molar ratio $gpA_1/gpNu1_2$. This terminase protomer possesses DNA maturation and packaging activities that are dependent on the *E. coli* integration host factor protein (IHF). Here, we show that the protomer further assembles into a homogeneous tetramer of protomers of composition $(gpA_1/gpNu1_2)_4$. Electron microscopy shows that the tetramer forms a ring structure large enough to encircle duplex DNA. In contrast to the heterotrimer, the ring tetramer can mature and package viral DNA in the absence of IHF. We propose that IHF induced bending of viral DNA facilitates the assembly of four terminase protomers into a ring tetramer that represents the catalytically competent DNA maturation and packaging complex *in vivo*. This work provides, for the first time, insight into the functional assembly state of a viral DNA packaging motor.

Terminase enzymes are common to double-stranded DNA (dsDNA) viruses that infect both prokaryotic and eukaryotic organisms (*1*−*6*). These enzymes function to insert a single viral genome into the interior of an empty procapsid, a process known as DNA packaging (*4*). For all viral systems that have been studied, the terminase holoenzyme is a heteroligomer composed of a large subunit that carries all of the catalytic activities required to package DNA and a small subunit that is responsible for specific recognition of the viral genome (*4*, *7*). The self-association reactions and the stoichiometries of the proteins assembled into these packaging motors remain poorly defined in all cases, however.

In bacteriophage λ, a dsDNA virus that infects *E. coli*, the preferred DNA packaging substrate, consists of a linear array of viral genomes linked in a head-to-tail fashion (a DNA concatemer). The cohesive end site (*cos*) is the junction between individual genomes in the concatemer and is the site where terminase assembles to initiate the packaging process (*3*, *4*, *6*). Lambda terminase is a heteroligomer composed of the viral gpA (73.3 kDa) and gpNu1 (20.4 kDa) proteins. The larger gpA protein possesses multiple enzymatic activities that are required to excise a single genome from the concatemer and concomitantly package it into the procapsid (see Figure 1) (*3*, *8*−*12*). These include site-specific *cos*-cleavage (endonuclease) activity, strand separation (helicase) activity, ATPase activity, and putative DNA translocation activity. The smaller gpNu1 protein has site-specific DNA binding activity and functions to recruit terminase to the *cos* site to initiate the packaging process (*13*−*16*).

We recently demonstrated that the two terminase proteins interact with each other, forming a stable and well-defined heterotrimeric complex that is composed of a dimer of gpNu1 tightly associated with a monomer of gpA ($gpA_1/gpNu1_2$) (*17*); we refer to this species as the terminase protomer[1]. The isolated protomer possesses *cos*-cleavage and DNA packaging activities that are strongly stimulated by IHF. The protomer also possesses weak ATPase activity. In addition to the protomer, the terminase isolated from overexpressing *E. coli* cell lines also forms a high-order complex composed of multiple gpA and gpNu1 proteins. This species possesses *cos* cleavage and DNA packaging activities that are independent of IHF (*17*). Moreover, the assembled complex possesses significant ATPase activity. The quaternary structure of this larger complex was not defined, however, because of the heterogeneity of the preparation (*17*).

In this work, we show that the isolated λ terminase protomer assembles into a stable, homogeneous, tetramer of protomers of composition $(gpA_1/gpNu1_2)_4$. Electron micros-

† This work was supported by National Institutes of Health Grants GM063943 (to C.E.C.) and GM51611 (to M.F.), a Kirschstein NRSA Postdoctoral Fellowship F32GM072349-01 (to N.K.M.), and by the Deutsche Forschungsgesellschaft BO1214/5-4 (to E.B.).

* To whom correspondence should be addressed. Tel: (206) 685-2468. Fax: (206) 685-3252. E-mail: catalanc@u.washington.edu.

‡ Department of Pharmaceutical Sciences, University of Colorado Health Sciences Center.

§ Molecular Biology Program, University of Colorado Health Sciences Center.

|| University of Iowa.

⊥ Friedrich-Alexander University.

Current address: Institut für Virology, Charité Universitätsmedizin Berlin, Charité Campus Mitte, Charitéplatz 1, 10117 Berlin, Germany.

[1] Abbreviations: Terminase protomer, a heterotrimer composed of one gpA associated with two gpNu1 proteins; Ring tetramer, assembly of four terminase protomers into a ring structure; VHW analysis, Van Holde-Weischet analysis; NLLS, non-linear least squares.

10.1021/bi0615036 CCC: $33.50 © 2006 American Chemical Society
Published on Web 11/30/2006

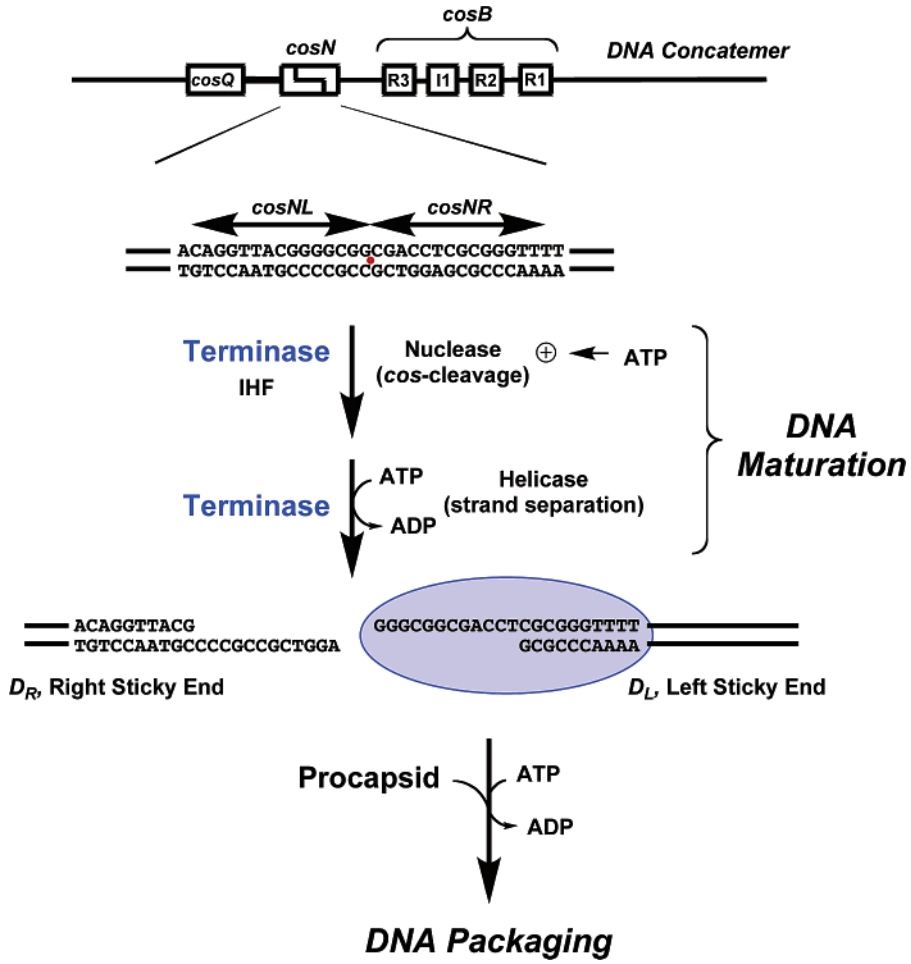

FIGURE 1: Schematic of λ terminase catalyzed DNA maturation reactions. *cos* represents the site where two individual λ genomes are linked head-to-tail in immature, concatemeric viral DNA. The *cos* site is subdivided into three functional regions, *cosQ*, *cosN*, and *cosB*, as shown. The terminase gpA subunit introduces symmetric nicks into the *cosN* subsite, and the resulting 12 base pairs of intervening DNA are separated by gpA's helicase activity. This matures the left genome end, generating the first complementary 5′ single stranded sticky end. λ terminase remains associated with the matured left end (D_L) forming complex I, which next binds to the portal complex, a ring structure located at a unique vertex of the procapsid. This activates ATPase activity of λ terminase, which translocates the DNA into the capsid. The assembly state of terminase in the DNA maturation and the packaging motor complexes remains unknown.

copy reveals that the tetramer forms a ring-like structure of sufficient size to encircle duplex DNA. Unlike the protomer, the ring tetramer possesses DNA maturation (*cos* cleavage endonuclease) and DNA packaging (virus assembly) activities that do not require IHF. Furthermore, the ring possesses ATPase activity that is over 3 orders of magnitude greater than that of the protomer. The implications of these results with respect to the nature of the DNA maturation and packaging motor complexes central to virus assembly are discussed.

EXPERIMENTAL PROCEDURES

Tryptone, yeast extract, and agar were purchased from DIFCO. Mature λ DNA was purchased from Invitrogen. Buffer A was made with doubly distilled water and contained 20 mM Tris at pH 8.65 at 4 °C, 300 mM NaCl, 5% (v/v) glycerol, and 0.1 mM EDTA. Lambda terminase was purified as described previously (*17*) and concentrated using an Amicon Ultra centrifugation concentration device (10,000 MWCO, Millipore). The concentration of the purified terminase preparation was determined by absorbance spectroscopy using an extinction coefficient of 1.57×10^5 M^{-1} cm^{-1}, and the molar ratio of gpNu1 to gpA was measured using SDS−PAGE followed by Commassie blue staining as described previously (*17*). Size exclusion gel chromatography utilized a HiPrep 16/60 Sephacryl S-300 column (~120 mL total volume, Pharmacia), which was developed with Buffer A at a flow rate of 0.3 mL/min, as described previously (*17*).

Sedimentation Velocity Experiments. Sedimentation velocity experiments were performed using protein that had eluted from the gel filtration column (HiPrep 16/60 Sephacryl S-300 HR from Pharmacia) using Buffer A as the running buffer. Protein samples (400 μL) were loaded into Epon charcoal-filled two sector centerpieces, and the running buffer was used for the reference chamber. Experiments were performed at 32,000 rpm, at 4 °C, using a Beckman XLA (Beckman Instruments, Inc., Fullerton, CA). Absorbance data were collected at 230 nm, using a spacing of 0.005 cm, with four averages in the continuous scan mode. Scans were collected every 2 min. The rotor, monochromator, and the chamber of the XLA were pre-chilled to 4 °C. Then the samples were loaded into the XLA, and the temperature was allowed to equilibrate to 4 °C prior to the initiation of an experiment. This process took about 1 h.

Sedimentation coefficients were corrected to standard conditions ($s_{20,w}$: 20 °C in water) using the program

SEDNTERP (David Hayes, Magdalen College; Tom Laue, University of New Hampshire; and John Philo, Amgen). Sample heterogeneity was assessed according to the Van Holde−Weischet method (*18*) using Borris Demeler's program Ultrascan (http://www.ultrascan.edu). The $g(s^*)$ distribution was calculated using DCDT+ (*19*), as described (*20*). To estimate the molecular weight of the higher order λ terminase complex, the raw sedimentation velocity traces were analyzed by nonlinear least-squares using Peter Schuck's program SEDFIT (*21*) (http://www.analyticalultracentrifugation.com/download.htm). SEDFIT solves the Lamm equation numerically, which allows estimation of both the sedimentation coefficient (by the rate of transport of the sample during sedimentation) and the diffusion coefficient (by the rate of boundary spreading during sedimentation) of the sample. With both of these parameters, the molecular weight can be calculated using the Svedberg equation (rearranged to solve for M):

$$M = \frac{sRT}{D(1 - \bar{v}\rho)} \quad (1)$$

where M is the molecular weight of the molecule, R is the gas constant, T is the temperature, s is the experimental sedimentation coefficient, D is the experimental diffusion coefficient, $\bar{v}$ is the partial specific volume of the molecule, and ρ is the density of the buffer. The weight averaged value of $\bar{v}$ was calculated from the primary sequences of gpA and gpNu1 according to the method of Cohn and Edsall (*22*), using a 2:1 molar ratio of gpNu1 to gpA (*17*). ρ was calculated using SEDNTERP.

Sedimentation Equilibrium Experiments. Sedimentation equilibrium experiments were performed using protein that had eluted from the gel filtration column with Buffer A as the running buffer. The protein was loaded into a chamber of an Epon charcoal-filled six-channel centerpiece, and the running buffer (Buffer A) was used for the reference chamber. The sample was sedimented to equilibrium at three rotor speeds, 7.5, 9, and 11 K rpm. The sample reached equilibrium within at least 24 h for each speed. Scans were collected at 227 nm and were taken every 0.001 cm in the step mode, with 20 averages per step.

The sedimentation equilibrium data were edited using an in-house program to extract the data between the sample meniscus and the bottom of the sample chamber for data analysis. The data were then analyzed using the nonlinear least-squares analysis program WINNONLIN (David Yphantis, University of Connecticut; Michael Johnson, University of Virginia; Jeff Lary, National Analytical Ultracentrifuge Center, Storrs, CT) to a single species model, given by:

$$A_T = \exp\left(\ln A_0 + \frac{M(1 - \bar{v}\rho)\omega^2}{2RT}(r^2 - r_0^2)\right) + b \quad (2)$$

where A_T is the total absorbance of the sample at radial position r, A_0 is the absorbance of the sample at the reference radial position r_0, M is the molecular weight of the sample, ω is the rotor speed, and b is the baseline offset. A_0 is taken into the exponent to implicitly constrain its domain to positive values.

Hydrodynamic Calculations. The frictional coefficient ratio, f/f_0, was calculated using:

$$\frac{f}{f_0} = \left(\frac{M^2(1 - \bar{v}\rho)^3}{162\pi^2(s_{20,w})^3\eta^3 N_A{}^2(\bar{v} + \delta v^0_{H20})}\right)^{1/3} \quad (3)$$

where η is the viscosity of pure water at 20 °C, N_A is Avogadro's number, ρ is the density of pure water at 20 °C, v^0_{H20} is the partial specific volume of pure water at 20 °C, and δ is the protein hydration in grams of water bound per gram of protein (*23*). δ was calculated on the basis of the primary sequences of gpNu1 and gpA associated in a 2:1 ratio using SEDNTERP according to the method of Kuntz (*24*), yielding a value of 0.4259 g/g.

Indirect Carbon Support Films. Carbon was evaporated from 1.0 mm carbon threat at a high of approximately 17 cm onto a glass slide. The carbon is reflected from the glass slide at an angle of 45° to a freshly cleaved mica in a coating unit with an operating vacuum of $<10^{-4}$ bar. Direct coating is prevented by a metal shield between the evaporation source and the mica.

Electron Microscopy. Purified protein (14.2 S species) was applied to the carbon on the mica and negative stained with 4% aqueous uranyl acetate (w/v) for 20 s. The stained protein was mounted on a 400 mesh copper grid, and micrographs were obtained using a Zeiss EM T109 electron microscope operated at a calibrated magnification (25,200×; by using a cross-ruled diffraction grating replica with 2.160 lines/mm (*25*)). Selected micrographs were digitized using a Microtex Scan Maker E6.

Terminase Activity Assays. The *cos*-cleavage endonuclease, ATPase and DNA packaging assays were conducted as previously described (*17*). The *in vitro* virus assembly plaque assay was performed as previously described (*26*) and is briefly described here. In this assay, an infectious virus is assembled entirely from purified components. The initial reaction mixtures contained 50 mM Tris at pH 8.0 at 4 °C, 2 mM spermidine, 10 mM $MgCl_2$, and 1 mM ATP. The virus was assembled in two stages. In the first stage, called the DNA packaging stage, 100 nM terminase, 2 nM mature λ DNA, 100 nM IHF, 10 μM gpFI, 50 nM procapsids, and 10 μM gpD were mixed and incubated at 22 °C for 20 min. The second stage, called the tail addition stage, was initiated by the addition of 10 mM gpFII, 10 μM gpW, and 50 nM tails, and the reactions were allowed to proceed for an additional 30 min at 37 °C. The infectious virus that was assembled in this mixture was quantified by the infection of *E. coli* LE392 using a standard plaque assay (*26*).

RESULTS

λ Terminase Protomer. Bacteriophage λ terminase, purified as described previously, affords a pure but heterogeneous mixture of higher-order, heteroligomeric species consisting of the gpNu1 and gpA proteins (*17*). Prior sedimentation velocity analysis of the mixture indicated that it has an average sedimentation coefficient ($s_{20,w}$) of 13.3 S, and for simplicity, we hereafter refer to it as the 13.3 S species. Dilution of the mixture in low salt buffer (Buffer A + 150 mM NaCl) followed by incubation at 4 °C for 2 days, as described in Experimental Procedures, promotes disassembly of ∼30% of the 13.3 S species into a stable terminase protomer that can be isolated by gel filtration chromatography (*17*). The isolated protomer possesses a [gpNu1]/[gpA] ratio of 2.0 ± 0.2, a molecular weight (M) of (115 ± 3), and an

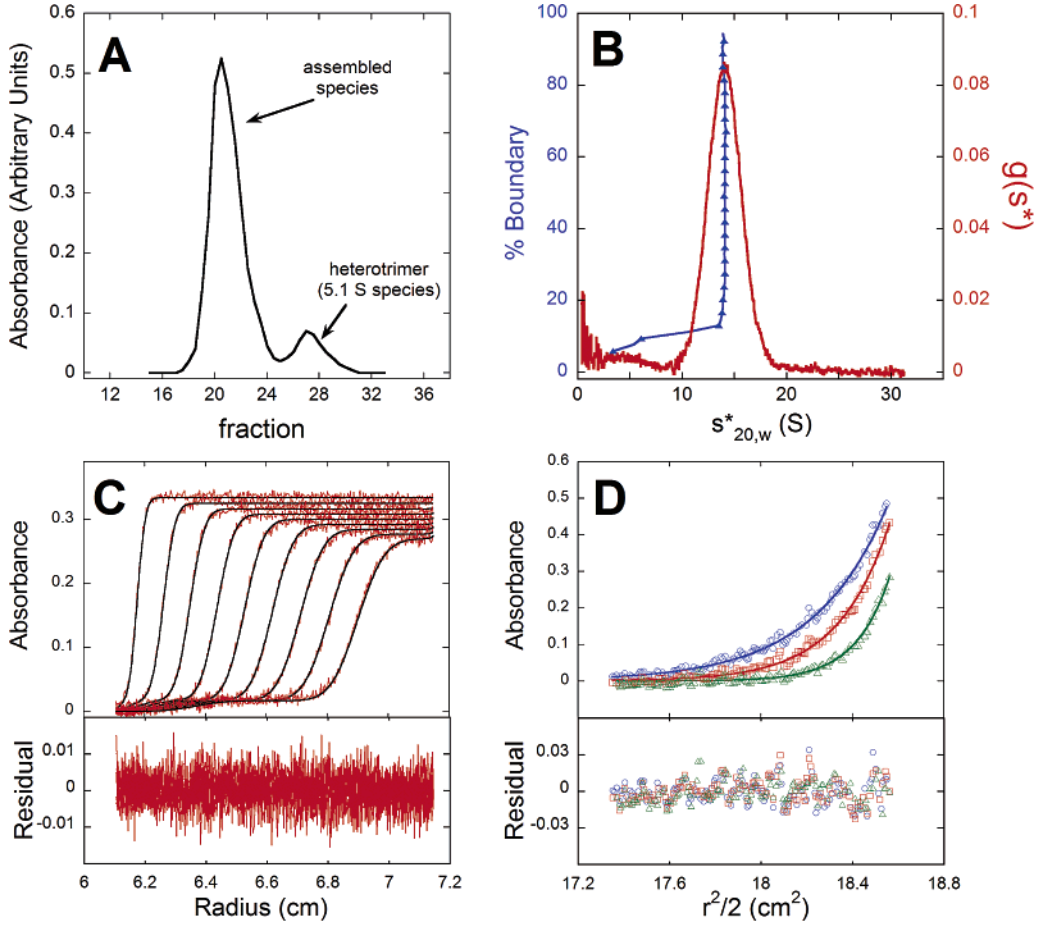

FIGURE 2: Assembly of λ terminase protomers. (Panel A) Size exclusion chromatographic analysis of the concentrated terminase protomer. The purified terminase heterotrimer was concentrated to 1.2 μM, then incubated at 4 °C for ~12 h. The sample (1 mL) was applied to an S300 HR sephacryl gel filtration column and developed with Buffer A. About 90% of the sample eluted as a single peak ahead of the heterotrimer peak (peak fraction 27). The assembled complex (fractions 18−23) was isolated for further study. (Panel B) Sedimentation velocity experiment performed using protein from the pooled fractions 18−23. The results from a Van Holde−Weischet (blue) and a *g*(s*) analysis (red) are shown. The vertical distribution of apparent sedimentation coefficients observed in the Van Holde−Weischet analysis and the symmetric nature of the *g*(s*) analysis indicate that the pooled protein is homogeneous. (Panel C) Analysis of the sedimentation velocity data to obtain the molecular weight of the 14 S species. The sedimentation velocity data were further analyzed by NLLS using the program SEDFIT to estimate the molecular weight of the species. The data were fit to a model that included two species, one of which corresponded to the small amount (5%) of the 5.1 S heterotrimer that was present in the sample; the other corresponded to the assembled species. This analysis returned a value of M = (459 ± 10) and a $s_{20,w}$ of (14.0 ± 0.2) S for the assembled species (average ± standard deviation for four independent experiments). (Panel D) Sedimentation equilibrium analysis of the associated terminase species. Protein from the pooled sample was subjected to a sedimentation equilibrium experiment. The sample was sedimented to equilibrium at 7.5 K (blue circles), 9 K (red squares) and 11K (green triangles) rpm, at 4 °C. The resulting profiles were globally analyzed by NLLS to a single ideal species model, which returned a molecular weight of (455 ± 45), consistent with the sedimentation velocity results.

$s_{20,w}$ of (5.12 S ± 0.03) S (*17*). These data unambiguously identify the protomer as a heterotrimer composed of one gpA subunit in association with a dimer of gpNu1 ($gpA_1/gpNu1_2$; predicted M = 114.2). Thus, the 13.3 S species provide a reliable source for a pure, homogeneous terminase protomer.

Purified λ Terminase Protomer Assembles into a Higher-Order Complex. We next examined the capacity of the terminase protomer to reassociate into a higher-order complex. The isolated protomer sample was concentrated in high-salt buffer (Buffer A + 300 mM NaCl; elevated [NaCl] promotes the assembly of higher-order structures (*17*)), incubated overnight at 4 °C, and then loaded onto a gel filtration column, as described in Experimental Procedures. The protein elutes from this column as two peaks (Figure 2A). The minor peak (fraction 27) corresponds to the protomer, whereas the majority (~90%, fraction 20) corresponds to a higher-order assembly of the protomer (see below). Column fractions 18−23 were pooled to facilitate the study of the assembled complex in isolation from the protomer.

We first determined the molar ratio of [gpNu1]/[gpA] in the assembled complex using an SDS−PAGE assay as described previously (*17*). This analysis gave 2.2 ± 0.2 for the oligomer, which is essentially identical to that found for the isolated protomer (2.0 ± 0.2; (*17*)). We interpret these data to indicate that the stoichiometry of the protomer is retained in the oligomeric complex.

Sedimentation Velocity Analysis of the Terminase Oligomer. We next performed sedimentation velocity experiments to determine the oligomeric state of the isolated, assembled terminase complex. Van Holde−Weischet (VHW) and g(s*) analysis of the data indicates that the protein preparation is composed primarily of a single species (>95%) with an $s_{20,w}$ of ~14 S (Figure 2B). Moreover, the vertical distribution of apparent sedimentation coefficients shows that the assembled complex is homogeneous, that is, composed of a single

Table 1: Physical Properties of the λ Terminase Oligomers

	13.3 S species	terminase protomer	terminase ring
protein purity	>98% pure	>98% pure	>98% pure
protein homogeneity	heterogeneous	homogeneous	homogeneous
[gpNu1]/[gpA]	2.8 ± 0.4	2.0 ± 0.2	2.2 ± 0.2
$s_{20,w}$	(13.30 ± 0.12) S	(5.12 ± 0.03) S	(14.0 ± 0.2) S
frictional ratio (f/f_o)		1.39 ± 0.01	1.28 ± 0.02
M (velocity)	(290 ± 13)	(115 ± 3)	(459 ± 10)
M (equilibrium)	(528 ± 34)	(116 ± 9)	(455 ± 45)
M (predicted)		114.2 (protomer)	456.8 (tetramer)

species that is not associating or dissociating on the time scale of the experiment (*27*). Thus, the data indicate that the 5.1 S protomer assembles into a homogeneous, higher-order oligomer with an $s_{20,w}$ value of ~14 S and that the two species do not interconvert on the time scale of a gel filtration (~4 h) or sedimentation velocity (~3 h) experiment.

Because the ~14 S species is homogeneous, the sedimentation velocity data can be analyzed directly to obtain the diffusion coefficient and, therefore, the molecular weight of the species (*17*, *21*, *28*). The sedimentation velocity profiles were analyzed by nonlinear least-squares (NLLS) analysis using the program SEDFIT (*21*), according to a two species model. This model was chosen in order to account for the small amount of protomer (5%) that is present in the preparation (Figure 2). The values for $s_{20,w}$ and *M* for the protomer were fixed at their previously determined values of 5.1 S and 115, respectively (*17*), and the NLLS analysis was performed as described in Experimental Procedures. An analysis of data obtained from four independent experiments performed with three different protein preparations yields best fit values of $s_{20,w} = (14.0 \pm 0.2)$ S and $M = (459 \pm 10)$ (average ± standard deviation) for the higher-order oligomer. The smooth curves that overlay the raw data in Figure 2C are simulations using the best-fit parameters derived from the NLLS analysis. These data combined with the known [gpNu1]/[gpA] ratio of 2.2 ± 0.2 (*vide supra*) unambiguously establish that the 14 S oligomer is composed of four terminase protomers, that is, a $(gpA/gpNu1_2)_4$ complex that has a predicted $M = 456.8$.

Sedimentation Equilibrium Analysis of the 14 S Terminase Oligomer. To confirm the results obtained in the sedimentation velocity experiments, the 14 S oligomer (200 nM gpA equivalents) was sedimented to equilibrium at three rotor speeds, 7.5, 9, and 11 K rpm; equilibrium was established within 24 h at each rotor speed. The concentration profiles were analyzed globally according to a single, ideal species model as described in Experimental Procedures, and the smooth curves that overlay the data in Figure 2D are simulations using the best-fit parameters from the analysis. The model describes the data well and returns a molecular weight of (455 ± 45), consistent with the value determined by sedimentation velocity (Table 1).

An analysis of the sedimentation velocity data indicates that the 14 S preparation contains 5% protomer species (Figure 2B and C), and it is feasible that this small amount of protomer might result in an underestimate of the fitted value of *M* when analyzing the sedimentation equilibrium data. To directly test this, we repeated the NLLS analysis explicitly assuming that the preparation contains 5% protomer. This analysis returns a value of $M = 460$, which is well within the experimental uncertainty of the measurement. Furthermore, fitting the data to more complex models does not improve the quality of the fit (not shown). Thus, the sedimentation equilibrium data confirm the sedimentation velocity data, and in sum, the AUC analysis demonstrates that the assembled terminase species is a tetramer of terminase protomers.

Electron Microscopy Analysis of the Terminase Oligomer. The 14 S terminase oligomer was analyzed by electron microscopy (EM) as described in Experimental Procedures, and a representative section is presented in Figure 3A. An inspection of the field shows that the molecules display a ring-shaped structure (Figure 3B). Image analysis allows an estimation of the ring dimensions and indicates that they have an overall width of ~19 nm and a height of ~22 nm. A central hole is visible in the structures, which on average is of sufficient size to encircle duplex DNA (~3 nm in diameter). On the basis of the results of the EM and AUC data, we refer to the 14 S species as a ring tetramer.

Hydrodynamic Properties of the Terminase Species. Analysis of sedimentation velocity data can also provide information on the shape of a macromolecule (*23*). The frictional coefficient of a hypothetical hydrated sphere of a given molecular weight and partial specific volume can be calculated (Experimental Procedures). This can be compared to the experimentally determined frictional coefficient of the protein of interest, in this case, the terminase species. The ratio of these two values yields the calculated frictional ratio, which can be interpreted in terms of the shape of the macromolecule: a frictional ratio close to one would suggest a compact globular structure, whereas a larger value would suggest that the molecule adopts an extended structure.

We first performed this analysis on the terminase protomer, which yields a calculated frictional ratio of 1.39 ± 0.01. This value is large and significantly greater than that expected for a compact, globular protein (*23*). This result indicates that the protomer structure is not globular but rather highly extended. Although this is often interpreted as molecular asymmetry, an alternate possibility is that one or both of the terminase proteins in the protomer possess partially disordered and/or unfolded regions; these regions would increase the frictional drag of the molecule, resulting in an increase in the measured frictional ratio.

Upon assembly of the protomer into the ring tetramer, the frictional ratio decreases to 1.28 ± 0.02. This observation indicates that the ring tetramer is more compact than the protomer, assuming the absence of significant differences in protein hydration between the two species. This may reflect large structural changes upon oligomerization, and it is tempting to speculate that disordered regions of the protomer fold upon assembly into the tetramer, resulting in a more compact structure.

Biological Activity of the Terminase Ring Tetramer. We previously demonstrated that the isolated terminase protomer possesses *cos*-cleavage activity and catalyzes DNA packaging *in vitro* but that both reactions are strongly stimulated by IHF (*17*). The heterogeneous 13.3 S species similarly catalyzes these reactions but does not require IHF. Furthermore, although the 13.3 S species possesses significant ATPase activity, ATP hydrolysis by the protomer is extremely weak. On the basis of these results, we proposed that IHF-induced bending of viral DNA is required to assemble the protomer into a packaging motor complex at

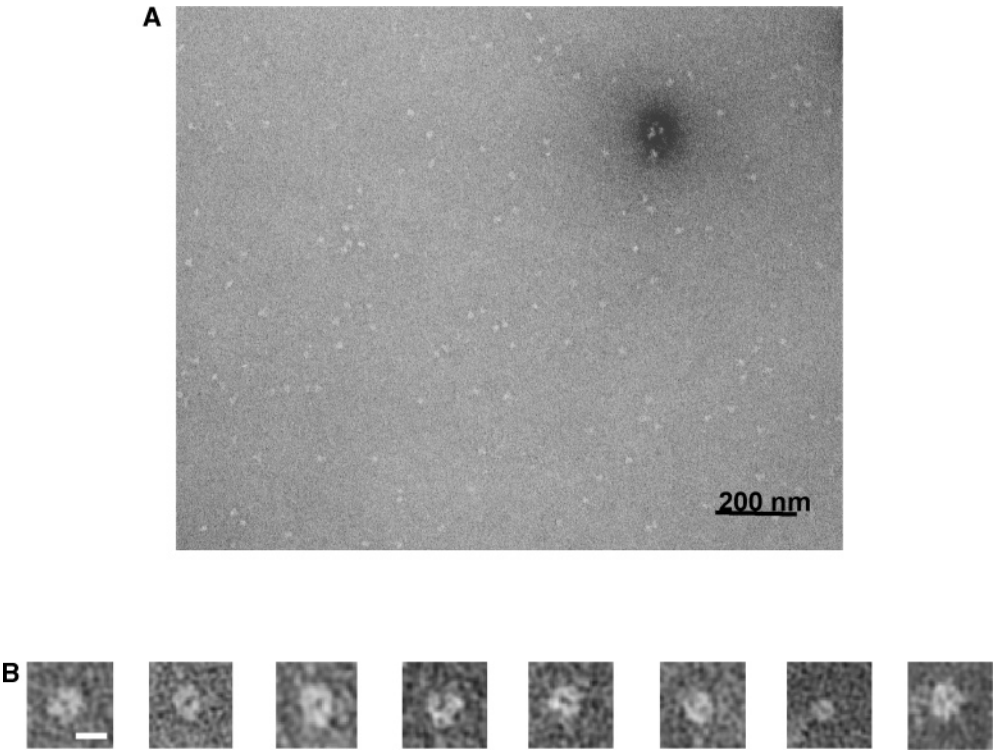

FIGURE 3: Electron micrographs of the λ terminase 14.0 S species. The 14.0 S terminase species was negatively stained with 4% (w/v) uranyl acetate and micrographs obtained as described in Experimental Procedures. (Panel A) Field of the 14.0 S terminase species. The bar is 200 nm. (Panel B) Gallery of individual ring species. The bar is 20 nm.

cos. In the case of the 13.3 S species, we proposed that a subpopulation of molecules is appropriately preassembled into an activated packaging motor and, therefore, does not require IHF to assemble on the DNA (*17*).

We recently developed an assay that allows the assembly of an infectious λ virus *in vitro* from purified components in a defined biochemical reaction mixture; virions thus assembled are quantified using a standard plaque assay (*26*). In contrast to the DNA packaging assay that only quantifies DNA rendered resistant to DNaseI digestion (*29*), the virus assembly assay reports on viral particles that have packaged the entire genome into the capsid and that have further assembled into a fully infectious virus. Here, we use this assay to compare the catalytic activities of the terminase protomer and the ring tetramer.

As shown in Figure 4, the terminase protomer (100 nM gpA equivalents) does not support the assembly of an infectious virus *in vitro* in the absence of IHF. On the basis of our previous results, this is likely the result of a failure of the protomer to package viral DNA (*17*). In the presence of 100 nM IHF, however, the terminase protomer efficiently packages the entire λ genome, leading to the formation of infectious virus particles in high yield. In contrast, if the protomer is preassembled into the ring tetramer (100 nM gpA equivalents), virus assembly proceeds efficiently in the absence of IHF. For comparison, Figure 4 also shows that the heterogeneous 13.3 S species similarly supports virus assembly in an IHF-independent manner, albeit at a lower efficiency. This observation is consistent with our previous suggestion that only a fraction of the 13.3 S species (20 to 30%) is correctly assembled into an active oligomeric state of the enzyme, presumably the 14.0 S ring tetramer.

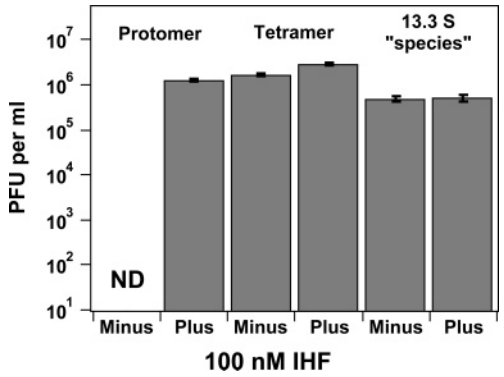

FIGURE 4: Catalytic activity of the λ terminase species. The *in vitro* virus assembly assay was performed as described in Experimental Procedures. The terminase species were added to a final concentration of 100 nM (gpA equivalents). IHF was included to a final concentration of 100 nM as indicated. ND, not detectable (<5 pfu/mL).

The *in vitro* virus assembly assay utilizes mature λ DNA and thus does not require nor measure the *cos*-cleavage activity of terminase holoenzyme. Therefore, we also tested the ability of the ring tetramer to catalyze the *cos*-cleavage endonuclease reaction. The ring tetramer efficiently cleaves *cos*-containing DNA in the absence of IHF (data not shown). This is in stark contrast to the *cos*-cleavage activity of the protomer, which is strongly stimulated by IHF (*17*). Furthermore, although the protomer possesses an extremely weak ATPase activity (*17*), the ring tetramer hydrolyzes ATP at a rate at least 3 orders of magnitude greater than that of the isolated heterotrimer ($k_{cat} = 50 \pm 2$ min^{-1} for the ring). Thus, the ring tetramer possesses all of the catalytic activities required to mature and package λ DNA, even in the absence of IHF.

DISCUSSION

Terminase enzymes are a core component of the genome packaging machinery in both prokaryotic and eukaryotic dsDNA viruses (*4*). Although structural characterization of the motors is limited in all of these systems, insight into the nature of the packaging motor in bacteriophage λ has been derived from studies of the individual subunits, as follows. Biochemical, biophysical, and structural studies have shown that the *N*-terminal 55 residues of the gpNu1 subunit comprise the DNA binding domain (DBD) of the protein (*30*−*32*). The DBD forms a stable dimer species that neither dissociates nor further associates over a wide concentration range (∼5 μM to 2 mM) (*30*−*32*). These data indicate that a gpNu1 dimer plays a functional role in DNA recognition and strongly suggest that the dimeric nature of gpNu1 is retained in the functional holoenzyme complex.

The terminase gpA subunit enhances the affinity of gpNu1 for *cos*-DNA (*16*), and it has long been appreciated that the functional holoenzyme is a heteroligomer of gpNu1 and gpA subunits. Genetic and biochemical studies have localized the holoenzyme interaction domains to the to the *C*-terminal ∼40 residues of gpNu1 and the *N*-terminal third of gpA (*15*, *33*−*35*). The oligomeric nature of the holoenzyme remained ambiguous, however, until our recent demonstration that a heterotrimer species is formed from the association a gpNu1 dimer with a single gpA protein ($gpA_1/gpNu1_2$, $s_{20,w} = 5.1$ S, $M = 115.3$) (*17*). The heterotrimer is stable and subunit dissociation is observed only under denaturing conditions. We interpret these data to indicate that a $gpA_1/gpNu1_2$ heterotrimer represents a terminase protomer and that this species is a core component of the catalytically competent holoenzyme complex.

Terminase Holoenzyme: A Ring Tetramer. The data presented here and in our previous publication (*17*) clearly demonstrate that the terminase protomer possesses *cos*-cleavage endonuclease, DNA packaging, and virus assembly activities that are strongly stimulated by IHF. We further show that the protomer associates into a tetrameric ring structure, off of the viral DNA, and that the tetramer possesses the full complement of catalytic activities in the absence of IHF. This *E. coli* host protein binds to a specific DNA recognition site and introduces a strong bend into the duplex. In all characterized cases, the IHF-induced bend provides a duplex architecture conducive to the assembly of additional proteins at that DNA site (*36*, *37*). Taken together, these data suggest that IHF binding to the I1 element of *cosB* (Figure 1) introduces a bend that facilitates the assembly of four terminase protomers into a catalytically competent DNA maturation and packaging complex. However, the ring tetramer represents a preassembled complex that can directly interact with the *cos* site in the absence of IHF.

Biochemical studies of terminase holoenzyme are consistent with the presence of an assembly step in the generation of a catalytically competent packaging complex as follows. (i) Kinetic analysis of the *cos*-cleavage reaction suggests that terminase assembly at the *cos* site is the rate-limiting step in the reaction (*38*, *39*). (ii) Kinetic studies have also shown that DNA stimulates the ATPase activity of terminase (*40*, *41*). The data presented here demonstrates that although the ring possesses significant ATPase activity, the protomer only poorly hydrolyzes ATP. We interpret these data to indicate that stimulation of ATPase activity results from the assembly of terminase protomers on duplex DNA. (iii) Vanadate inhibits the nuclease, helicase, ATPase, and DNA packaging activities of the terminase holoenzyme (*42*). A detailed kinetic analysis of this inhibition suggests that DNA and ADP act in concert to assemble a catalytically competent DNA maturation and packaging complex at the *cos* site (*42*). (iv) DNase protection studies have shown that in the absence of ATP, terminase protects only the three R-elements of *cosB* (Figure 1). In the presence of ATP, however, terminase interacts with roughly 200 bp of DNA centered at the *cos* site (*13*). The authors interpreted these data to indicate that ATP drives the assembly of "an organized protein·DNA complex involving several terminase protomers". In sum, the published data and that presented here are consistent with a DNA, IHF, and ATP regulated assembly step that is required to activate terminase holoenzyme. We propose that this step reflects the assembly of four terminase protomers into a ring-like structure that bends and wraps *cos*-DNA. We further suggest that the ring tetramer represents the activated nuclease complex characterized in kinetic studies (*42*) and is directly responsible for the packaging of the λ genome.

How Might a Ring Tetramer Assemble? To address this question, we rely on a variety of published information, as follows. (i) Mutation analysis of the *cosN* site revealed an asymmetry in the *cos*-cleavage reaction (*43*). The data suggest that terminase assembly at *cos* is mediated by intrinsic binding interactions between the gpA subunits and their respective *cosN* half-sites and, less critically, by cooperative binding interactions between the gpA subunits. Furthermore, the assembly of gpA at the *cosNR* half-site is strongly influenced by cooperative binding interactions of gpNu1 and *cosB*. Thus, it is clear that terminase assembly at *cos* is mediated by both protein−protein and protein−DNA interactions. (ii) Primary sequence analysis has identified a basic leucine zipper (bZIP) protein dimerization motif in the *C*-terminal region of gpA (residues 560−620) (*44*). This bipartite protein dimerization-DNA binding motif is composed of a region enriched in basic amino acids (basic region) adjacent to a coiled coil leucine zipper motif (*44*). The dimerization of bZIP-containing proteins via their coiled coil motifs is supported by cooperative interactions between the basic protein residues and the phosphate groups of duplex DNA. It has long been presumed that bZIP residues mediate the assembly of a symmetrically disposed gpA dimer at the *cosN* site and that this dimer is directly responsible for the symmetric nicking of the duplex (*44*). We suggest that the bZIP protein−protein interaction is central to the assembly of the ring tetramer, both on and off DNA. (iii) Biochemical data has shown that although the gpNu1 DBD retains DNA binding activity, specific and high affinity binding interactions require a hydrophobic self-association domain of the protein (residues 101−141); deletion of these residues decreases DNA binding affinity by 3 orders of magnitude (*35*). This observation suggests that higher-order interactions are required for specific and high affinity binding of gpNu1 at the *cosB* site. Consistently, primary sequence analysis has identified coiled coil protein dimerization motifs within the *C*-terminal half of gpNu1 (*45*). It is likely the coiled coil motifs, together with the hydrophobic self-association domains of gpNu1, are involved in the assembly of the ring tetramer. Therefore, we propose that terminase protomers

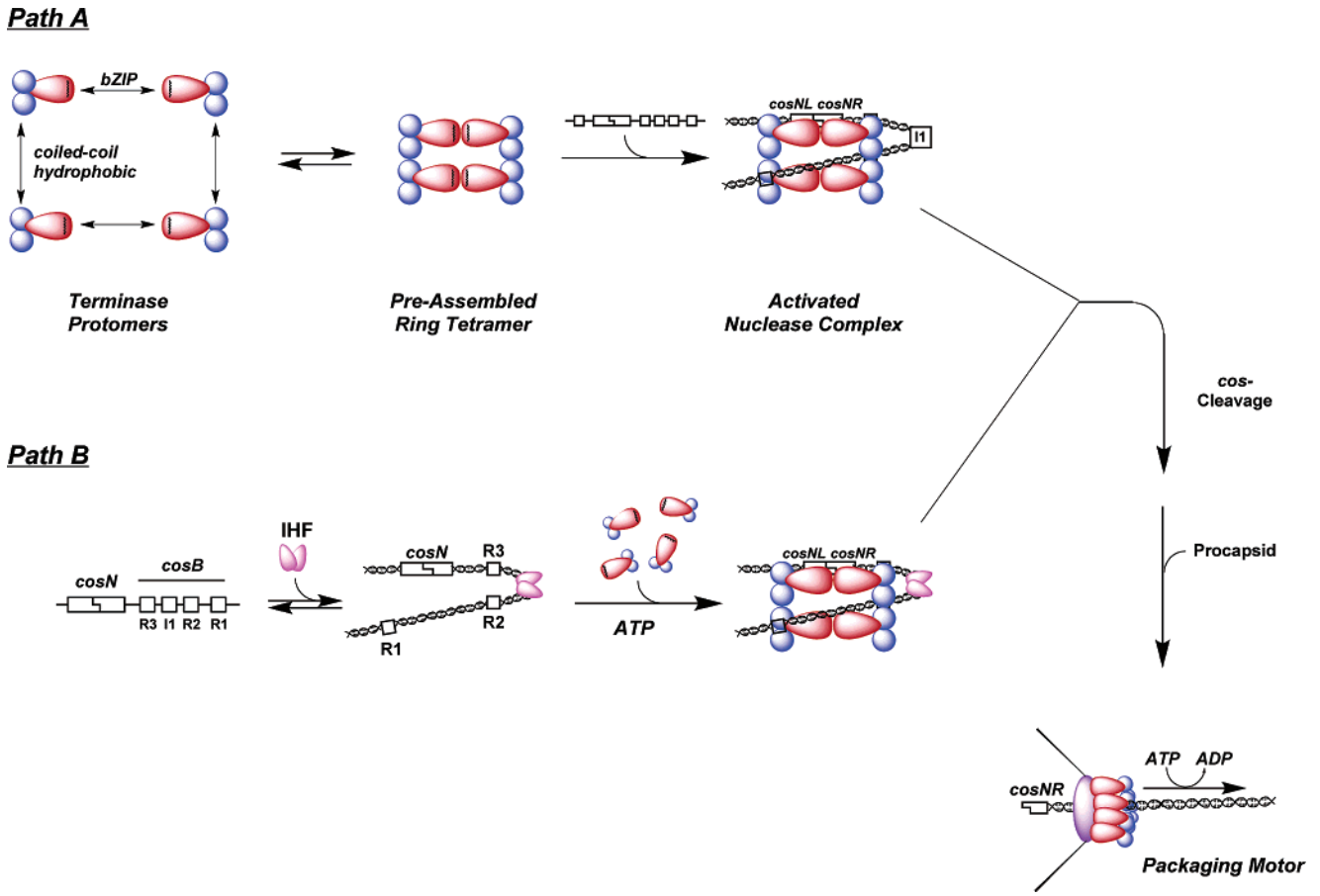

FIGURE 5: Assembly of λ terminase protomers into DNA maturation and DNA packaging motor complexes. (Path A) The terminase protomer preassembles into a ring tetramer that binds directly to the *cos* site, independent of *E. coli* IHF. (Path B) IHF binds to the *cos* site and introduces a strong bend into the duplex, which provides an architecture conducive to the assembly of a terminase ring structure. The *E. coli* HU protein may also bind to the pre-bent I1 element and bend the duplex in a manner analogous to that of IHF. The details are presented in the text.

associate with each other in two distinct ways: first, through the bZIP dimerization motif in the *C*-terminal region of gpA and second, through the coiled coil dimerization motifs found within the hydrophobic self-association domain of gpNu1.

Biological Significance of the Terminase Ring Tetramer. To date, there is limited information describing the structure or self-association reactions for a terminase enzyme from any viral system. We have shown that a stable λ terminase protomer is formed from one gpA subunit in association with a gpNu1 dimer and that the protomer further assembles into a ring tetramer in which the DNA maturation and packaging activities of the enzyme are fully activated. These data strongly suggest, but do not unambiguously prove, that the tetramer is the biologically relevant form of the enzyme. It is feasible, for instance, that the ring dissociates and subsequently reassembles into a different complex on viral DNA. We think this is unlikely, however, because of the stability of the ring once it is formed ($t_{1/2} \geq 72$ h). Another possibility is that multiple ring tetramers are required for DNA maturation and/or packaging activities, as has been observed for the SV40 large T antigen and the MCM helicase (*46*, *47*). Whatever the case, it is clear that assembly of the ring tetramer obviates the IHF requirement for catalysis, demonstrating at a minimum that it is an important intermediate in the DNA maturation and packaging reactions.

How Does the Terminase Ring Assemble in Vivo? Two obvious pathways need to be considered. The first involves preassembly of protomers into the ring tetramer in the absence of DNA followed by direct binding to the *cos* site in an IHF-independent process (Figure 5, Path A). The data presented here clearly indicate that a functional ring tetramer can be assembled *in vitro* and that this complex possesses catalytic activity in the absence of IHF; however, elevated protein concentrations (>1 μM) and high salt (300 mM) are required to assemble the complex. The concentration of terminase during a productive infection is comparatively low (~150 nM gpA subunit) (*26*), which predicts that only small amounts of the ring will form *in vivo*. Thus, the second pathway that needs to be considered is the assembly of four terminase protomers into a ring, mediated by *cos* DNA and IHF (Figure 5, Path B). Given the concentration of terminase present in the cell (*vide supra*), one would expect Path B to dominate *in vivo*. Consistent with this assertion, λ burst sizes are reduced ~3-fold in IHF$^-$ cell lines and by over 2 orders of magnitude in IHF$^-$/HU$^-$ double mutant cell lines (*36*). *E. coli* HU is a nonspecific DNA binding and bending protein with structural similarity to IHF. Within this context, it is noteworthy that the I1 element within *cosB* is intrinsically bent (*48*) and that HU has a higher affinity for pre-bent DNA duplexes (*49*). It is thus likely that HU specifically recognizes this site and introduces additional bending into the duplex

appropriately positioned within *cos*. In this manner, the HU protein may substitute for IHF to provide a duplex architecture conducive to the assembly of a ring tetramer (Figure 5).

λ Terminase and the Packaging Motor. It has been argued that a symmetrically disposed gpA dimer assembles at *cosN* to nick the duplex and mature the genome end (*44*). In contrast, it has been presumed that the packaging motor complex is composed of a hexameric gpA ring bound to the portal vertex (*50*). Integration of these two concepts into a coherent model describing the packaging pathway has been difficult and has led to cumbersome models describing the transition from a nuclease dimer to a hexameric motor complex (*4*). The concept of a catalytically competent terminase ring structure that is responsible for both DNA maturation and packaging activities allows for a simplified model as presented in Figure 5. The nature of the packaging complexes remains vague in all viral systems, but it is reasonable to assume that the *bona fide* motors are composed of both terminase and portal proteins. The terminase ring tetramer characterized here presents a central cavity of sufficient size to encircle duplex DNA and whose dimensions, to the first approximation, match those measured in several portal structures (*51*). Embracing of the viral DNA by both the terminase ring and the portal ring would engender a tightly bound, highly processive packaging motor complex that could translocate the entire genome into the capsid in a single DNA binding event. Indeed, single molecule studies of DNA packaging in the bacteriophage ϕ29 system indicate that the genome packaging motor is extremely powerful and that the packaging process is highly processive (*52*).

Mechanistic Implications for Viral DNA Packaging Motors. It is likely that the general features herein described for the λ terminase holoenzyme are recapitulated in the other viral systems and that highly processive ring structures are a fundamental aspect of the packaging motors. Indeed, cryoEM reconstructions of bacteriophage ϕ29 capsids captured in the process of packaging DNA suggest that a ring complex might be part of the packaging motor in this virus (*53*). A small packaging RNA (pRNA) is integral to the packaging process in ϕ29, and the reconstructions clearly show 5-fold symmetric RNA density associated with the portal vertex. Additional density at the packaging vertex is also observed, and the authors suggest that this may be attributed to the protein component of the packaging motor, that is, terminase. This density similarly shows apparent 5-fold symmetry, but this is not unanticipated because the structure was obtained by imposing 5-fold symmetry along the particle axis (*53*). Whatever the case, the authors suggest that a pentameric pRNA ring is anchored to the capsid vertex and that each subunit of the pRNA is attached to a terminase monomer; this model thus predicts that terminase possesses 5-fold symmetry co-incident with the pRNA. In contrast, the data presented here suggest that the lambda packaging motor corresponds to a ring structure composed of four terminase protomers.

The stoichiometry of terminase protomers assembled into the packaging complexes has direct implications on the mechanism by which these motors translocate DNA into the capsid. It has long been argued that a symmetry mismatch between the portal (12 fold) and the capsid vertex (5 fold) would result in a reduction in the activation barrier of rotation of the portal (*54*). On the basis of this concept, it was proposed that portal rotation relative to the capsid vertex is coupled to linear translocation of the DNA into the capsid. The terminase enzymes directly interact with the portals in the packaging complexes, and the symmetry of this interaction must be considered in models describing the translocation process. A pentameric terminase complex presents a symmetry mismatch relative to the portal, and successive firing of the terminase ATPase could then drive the rotation of the portal, relative to the terminase ring, resulting in packaging of the DNA. In contrast, a tetrameric terminase ring presents a symmetric interface to the portal, which predicts that the terminase ring remains in register with the portal ring during the entirety of the packaging process. Unfortunately, the molecular details of DNA translocation by the terminase packaging motors remain uncertain at present and must await further biochemical and structural dissection.

ACKNOWLEDGMENT

We thank Dr. Qin Yang for help with the virus assembly assay and additional technical expertise. In addition, we thank Drs. Yang and David Bain for helpful discussions.

REFERENCES

1. Black, L. W. (1989) DNA packaging in dsDNA bacteriophages, *Annu. Rev. Microbiol. 43*, 267−292.
2. Casjens, S. (1985) *Virus Structure and Assembly*, Jones and Bartlett, Boston, MA.
3. Catalano, C. E. (2000) The terminase enzyme from bacteriophage lambda: a DNA-packaging machine, *Cell. Mol. Life Sci. 57*, 128−148.
4. Catalano, C. E. (2005) *Viral Genome Packaging Machines: Genetics, Structure, and Mechanism*, Landes Bioscience/Eurekah.com, Kluwer Academic/Plenum Publishers, Georgetown, TX.
5. Grimes, S., Jardine, P. J., and Anderson, D. (2002) Bacteriophage phi 29 DNA packaging, *Adv. Virus Res. 58*, 255−294.
6. Murialdo, H. (1991) Bacteriophage lambda DNA maturation and packaging, *Annu. Rev. Biochem. 60*, 125−153.
7. Fujisawa, H., and Morita, M. (1997) Phage DNA packaging, *Genes Cells 2*, 537−545.
8. Duffy, C., and Feiss, M. (2002) The large subunit of bacteriophage lambda's terminase plays a role in DNA translocation and packaging termination, *J. Mol. Biol. 316*, 547−561.
9. Hang, J. Q., Tack, B. F., and Feiss, M. (2000) ATPase center of bacteriophage lambda terminase involved in post-cleavage stages of DNA packaging: identification of ATP-interactive amino acids, *J. Mol. Biol. 302*, 777−795.
10. Hwang, Y., and Feiss, M. (1996) Mutations affecting the high affinity ATPase center of gpA, the large subunit of bacteriophage lambda terminase, inactivate the endonuclease activity of terminase, *J. Mol. Biol. 261*, 524−535.
11. Rubinchik, S., Parris, W., and Gold, M. (1994) The in vitro endonuclease activity of gene product A, the large subunit of the bacteriophage lambda terminase, and its relationship to the endonuclease activity of the holoenzyme, *J. Biol. Chem. 269*, 13575−13585.
12. Rubinchik, S., Parris, W., and Gold, M. (1995) The in vitro translocase activity of lambda terminase and its subunits. Kinetic and biochemical analysis, *J. Biol. Chem. 270*, 20059−20066.
13. Higgins, R. R., and Becker, A. (1995) Interaction of terminase, the DNA packaging enzyme of phage lambda, with its *cos* DNA substrate, *J. Mol. Biol. 252*, 31−46.
14. Shinder, G., and Gold, M. (1988) The Nul subunit of bacteriophage lambda terminase binds to specific sites in *cos* DNA, *J. Virol. 62*, 387−392.
15. Yang, Q., Berton, N., Manning, M. C., and Catalano, C. E. (1999) Domain structure of gpNu1, a phage lambda DNA packaging protein, *Biochemistry 38*, 14238−14247.

16. Yang, Q., Hanagan, A., and Catalano, C. E. (1997) Assembly of a nucleoprotein complex required for DNA packaging by bacteriophage lambda, *Biochemistry 36*, 2744−2752.
17. Maluf, N. K., Yang, Q., and Catalano, C. E. (2005) Self-association properties of the bacteriophage lambda terminase holoenzyme: implications for the DNA packaging motor, *J. Mol. Biol. 347*, 523−542.
18. Demeler, B., and van Holde, K. E. (2004) Sedimentation velocity analysis of highly heterogeneous systems, *Anal. Biochem. 335*, 279−288.
19. Philo, J. S. (2000) A method for directly fitting the time derivative of sedimentation velocity data and an alternative algorithm for calculating sedimentation coefficient distribution functions, *Anal. Biochem. 279*, 151−163.
20. Stafford, W. F., III. (1992) Boundary analysis in sedimentation transport experiments: a procedure for obtaining sedimentation coefficient distributions using the time derivative of the concentration profile, *Anal. Biochem. 203*, 295−301.
21. Schuck, P. (1998) Sedimentation analysis of noninteracting and self-associating solutes using numerical solutions to the Lamm equation, *Biophys. J. 75*, 1503−1512.
22. Laue, T. M. (1995) Sedimentation equilibrium as thermodynamic tool, *Methods Enzymol. 259*, 427−452.
23. Tanford, C. (1961) *Physical Chemistry of Macromolecules*, Wiley, New York.
24. Kuntz, I. D. (1971) Hydration of macromolecules. IV. Polypeptide conformation in frozen solutions, *J. Am. Chem. Soc. 93*, 516−518.
25. Bozzola, J. J., Russell, L. D., and NetLibrary, Inc. (1999) Jones and Bartlett, Sudbury, MA.
26. Gaussier, H., Yang, Q., and Catalano, C. E. (2006) Building a virus from scratch: assembly of an infectious virus using purified components in a rigorously defined biochemical assay system, *J. Mol. Biol. 357*, 1154−1166.
27. Demeler, B., Saber, H., and Hansen, J. C. (1997) Identification and interpretation of complexity in sedimentation velocity boundaries, *Biophys. J. 72*, 397−407.
28. Schuck, P. (2003) On the analysis of protein self-association by sedimentation velocity analytical ultracentrifugation, *Anal. Biochem. 320*, 104−124.
29. Yang, Q., and Catalano, C. E. (2003) Biochemical characterization of bacteriophage lambda genome packaging in vitro, *Virology 305*, 276−287.
30. Bain, D. L., Berton, N., Ortega, M., Baran, J., Yang, Q., and Catalano, C. E. (2001) Biophysical characterization of the DNA binding domain of gpNu1, a viral DNA packaging protein, *J. Biol. Chem. 276*, 20175−20181.
31. de Beer, T., Fang, J., Ortega, M., Yang, Q., Maes, L., Duffy, C., Berton, N., Sippy, J., Overduin, M., Feiss, M., and Catalano, C. E. (2002) Insights into specific DNA recognition during the assembly of a viral genome packaging machine, *Mol. Cell. 9*, 981−991.
32. Gaussier, H., Ortega, M. E., Maluf, N. K., and Catalano, C. E. (2005) Nucleotides regulate the conformational state of the small terminase subunit from bacteriophage lambda: implications for the assembly of a viral genome-packaging motor, *Biochemistry 44*, 9645−9656.
33. Frackman, S., Siegele, D. A., and Feiss, M. (1985) The terminase of bacteriophage lambda. Functional domains for *cosB* binding and multimer assembly, *J. Mol. Biol. 183*, 225−238.
34. Wu, W. F., Christiansen, S., and Feiss, M. (1988) Domains for protein-protein interactions at the N and C termini of the large subunit of bacteriophage lambda terminase, *Genetics 119*, 477−484.
35. Yang, Q., de Beer, T., Woods, L., Meyer, J. D., Manning, M. C., Overduin, M., and Catalano, C. E. (1999) Cloning, expression, and characterization of a DNA binding domain of gpNu1, a phage lambda DNA packaging protein, *Biochemistry 38*, 465−477.
36. Mendelson, I., Gottesman, M., and Oppenheim, A. B. (1991) HU and integration host factor function as auxiliary proteins in cleavage of phage lambda cohesive ends by terminase, *J. Bacteriol. 173*, 1670−1676.
37. Rice, P. A., Yang, S., Mizuuchi, K., and Nash, H. A. (1996) Crystal structure of an IHF-DNA complex: a protein-induced DNA U-turn, *Cell 87*, 1295−1306.
38. Tomka, M. A., and Catalano, C. E. (1993) Kinetic characterization of the ATPase activity of the DNA packaging enzyme from bacteriophage lambda, *Biochemistry 32*, 11992−11997.
39. Woods, L., Terpening, C., and Catalano, C. E. (1997) Kinetic analysis of the endonuclease activity of phage lambda terminase: assembly of a catalytically competent nicking complex is rate-limiting, *Biochemistry 36*, 5777−5785.
40. Tomka, M. A., and Catalano, C. E. (1993) Physical and kinetic characterization of the DNA packaging enzyme from bacteriophage lambda, *J. Biol. Chem. 268*, 3056−3065.
41. Woods, L., and Catalano, C. E. (1999) Kinetic characterization of the GTPase activity of phage lambda terminase: evidence for communication between the two "NTPase" catalytic sites of the enzyme, *Biochemistry 38*, 14624−14630.
42. Yang, Q., and Catalano, C. E. (2004) A minimal kinetic model for a viral DNA packaging machine, *Biochemistry 43*, 289−299.
43. Hang, J. Q., Catalano, C. E., and Feiss, M. (2001) The functional asymmetry of *cosN*, the nicking site for bacteriophage lambda DNA packaging, is dependent on the terminase binding site, *cosB*, *Biochemistry 40*, 13370−13377.
44. Davidson, A. R., and Gold, M. (1992) Mutations abolishing the endonuclease activity of bacteriophage lambda terminase lie in two distinct regions of the A gene, one of which may encode a "leucine zipper" DNA-binding domain, *Virology 189*, 21−30.
45. Kondabagil, K. R., and Rao, V. B. (2006) A critical coiled coil motif in the small terminase, gp16, from bacteriophage T4: insights into DNA packaging initiation and assembly of packaging motor, *J. Mol. Biol. 358*, 67−71.
46. Fletcher, R. J., Shen, J., Gomez-Llorente, Y., Martin, C. S., Carazo, J. M., and Chen, X. S. (2005) Double hexamer disruption and biochemical activities of Methanobacterium thermoautotrophicum MCM, *J. Biol. Chem. 280*, 42405−42410.
47. Li, D., Zhao, R., Lilyestrom, W., Gai, D., Zhang, R., DeCaprio, J. A., Fanning, E., Jochimiak, A., Szakonyi, G., and Chen, X. S. (2003) Structure of the replicative helicase of the oncoprotein SV40 large tumour antigen, *Nature 423*, 512−518.
48. Yeo, A., Kosturka, L. D., and Feiss, M. (1990) Structure of the bacteriophage lambda cohesive end site: bent DNA on both sides of the site, *cosN*, at which terminase introduces nicks during chromosome maturation, *Virology 174*, 329−334.
49. Wojtuszewski, K., and Mukerji, I. (2003) HU binding to bent DNA: a fluorescence resonance energy transfer and anisotropy study, *Biochemistry 42*, 3096−3104.
50. Catalano, C. E., Cue, D., and Feiss, M. (1995) Virus DNA packaging: the strategy used by phage lambda, *Mol. Microbiol. 16*, 1075−1086.
51. Valpuesta, J. M., and Carrascosa, J. L. (1994) Structure of viral connectors and their function in bacteriophage assembly and DNA packaging, *Q. Rev. Biophys. 27*, 107−155.
52. Smith, D. E., Tans, S. J., Smith, S. B., Grimes, S., Anderson, D. L., and Bustamante, C. (2001) The bacteriophage straight phi29 portal motor can package DNA against a large internal force, *Nature 413*, 748−752.
53. Simpson, A. A., Tao, Y., Leiman, P. G., Badasso, M. O., He, Y., Jardine, P. J., Olson, N. H., Morais, M. C., Grimes, S., Anderson, D. L., Baker, T. S., and Rossmann, M. G. (2000) Structure of the bacteriophage phi29 DNA packaging motor, *Nature 408*, 745−750.
54. Hendrix, R. W. (1978) Symmetry mismatch and DNA packaging in large bacteriophages, *Proc. Natl. Acad. Sci. U.S.A. 75*, 4779−4783.

BI0615036